PHYSICAL REVIEW B **97**, 165420 (2018)

Electrochemical capacitance modulation in an interacting mesoscopic capacitor induced by internal charge transfer

Wei Liu,[1] Jianhong He,[1] Huazhong Guo,[1] and Jie Gao[1,2,*]
[1]*Department of Physics, Sichuan University, Chengdu 610064, People's Republic of China*
[2]*National Institute of Measurement and Testing Technology, Chengdu 610021, People's Republic of China*

(Received 24 October 2017; revised manuscript received 30 March 2018; published 16 April 2018)

We report experiments on the dynamic response of an interacting mesoscopic capacitor consisting of a quantum dot with two confined spin-split levels of the lowest Landau level. In high magnetic fields, states inside the dot are regulated by a mixture of Coulomb interaction and Landau-level quantization, and electrons distribute on two spatially separated regions. Quantum point contact voltage and magnetic field are employed to manipulate the number and distribution of electrons inside the quantum dot. We find that the periodicity of the electrochemical capacitance oscillations is dominated by the charging energy, and their amplitudes, due to internal charge transfer and strong internal capacitive coupling, show rich variations of modulations. Magnetocapacitance displays a sawtoothlike manner and may differ in tooth directions for different voltages, which, we demonstrate, result from a sawtoothlike electrochemical potential change induced by internal charge transfer and field-sensitive electrostatic potential. We further build a charge stability diagram, which, together with all other capacitance properties, is consistently interpreted in terms of a double-dot model. The demonstrated technique is of interest as a tool for fast and sensitive charge state readout of a double-quantum-dot qubit in the gigahertz frequency quantum electronics.

DOI: 10.1103/PhysRevB.97.165420

I. INTRODUCTION

Recent experimental development in high-frequency ac transport has enabled us to investigate the dynamics of a mesoscopic capacitor [1–4]. The capacitor, similar to a standard parallel-plate capacitor, consists of a submicrometer quantum dot (QD) and a macroscopic metallic top gate, each acting as one plate. The QD is linked to a wide two-dimensional electron gas (2DEG) reservoir through a single-channel narrow constriction formed by a quantum point contact (QPC). One remarkable difference, compared to a two-metallic-plate capacitor, is that electric field can penetrate the 2DEG before being completely screened due to low density of electron. Consequently, quantum capacitance, closely related to the density of states inside the dot, has to be introduced in addition to the geometric capacitance. Capacitance measurements, hence, provide a powerful tool to probe the internal device properties [5] as well as anomalous Coulomb correlation effects [6–9]. One major advantage of this capacitor, compared to former mesoscopic devices, is that the dynamic effects provide the leading order of the system response, as the dc transport is completely suppressed. It allows us to fast manipulate and read off the electron states inside the dot, which is an important requirement in any quantum information processing scheme. Operated out of equilibrium by a fast voltage modulation, on-demand single electron source [2], which emits the electrons into a well-defined quantum state, has been realized, and new generation devices based on this capacitor, in close analogy to quantum optic apparatuses, have been utilized to investigate coherent ballistic electronic transport [4,10–12].

Of fundamental interest about this system is its low-frequency linear response, which is well described [1,13] by a series connection of a charge relaxation resistance R_q and an electrochemical capacitance C_μ, and the ac impedance of the system is

$$Z(\omega) = R_q + \frac{1}{i\omega C_\mu}, \tag{1}$$

where $\omega/2\pi$ is the radio-frequency (rf) excitation frequency. The first term on the right is the charge relaxation resistance R_q, i.e., the dissipative element, which was found by a recent experiment [1] to be universal as a quantized value $h/2e^2$. The second term gives access to the electrochemical capacitance C_μ, i.e., the reactive element, which is closely related to the density of states but its properties have not been carefully established in earlier experiments [1,3]. However, C_μ, together with R_q, defines a characteristic timescale, i.e., the charge relaxation time $\tau_{RC} = R_q C_\mu$, which plays a central role in the dynamics of single electrons [3,14,15]. Moreover, for high excitation frequency ($\omega/2\pi > 1/\tau_{RC}$), the electrochemical capacitance was predicted to become negative due to slow charge relaxation [16,17]. Therefore, the electrochemical capacitance not only serves as a sensitive detection method for the internal properties of quantum conductors and controls the charge relaxation process inside them, but also in itself is a very significative quantity in quantum coherent electronics and worth further experimental investigations, in particular, at gigahertz frequencies.

On the other hand, most experiments [1,3,18] have mainly focused on the weak interacting regime where the charging

---

[*] gaojie@scu.edu.cn

energy is negligibly small compared to the orbital level spacing. However, small-sized QDs often exhibit strong Coulomb blockade effects, and it is, therefore, desirable to ask what would happen under this condition. Numerous theoretical works [19–23] addressed the dynamic properties of this capacitor in the strong interaction regime. Remarkably, they found that the charge relaxation resistance is not affected and is still universal [19–21]. However, the electrochemical capacitance, in contrast, was predicted to sensitively depend on the Coulomb interaction [22], as the dot density of states at the Fermi energy is tremendously modified by the charging energy. Furthermore, self-consistent calculations [24,25] show that charges inside the QD distribute in spatially separated compressible regions and they can transfer between these regions by tunneling. This internal charge redistribution can change the charging energy of the dot and has been demonstrated experimentally to modulate the dc conductance [24,26]. Several theoretical works [27,28] also predicted that the capacitance is sensitive to the charge redistribution as well, however, a systematic experimental study of the electrochemical capacitance in this strong interacting regime is still lacking.

Here, we report experimental measurements of the electrochemical capacitance on an interacting mesoscopic capacitor in the quantum Hall regime. We focus on the weak tunneling regime where only one spin-split channel is partly open and quantization of electrons on the dot is well defined. We manipulate the number of electrons and their distributions inside the QD by the QPC voltage and the magnetic field. We find that both the periodicity and amplitudes of the electrochemical capacitance oscillations are modified by the charging energy and the internal electron distribution when V_{QPC} is varied. Electrochemical capacitance C_μ displays a sawtoothlike behavior when the magnetic field is employed to rearrange the charge distribution in the QD. A two-dot model calculation that considers the interactions between different regions inside the quantum dot is employed to understand these exotic electrochemical capacitance behaviors.

The paper is organized as follows. In Sec. II, we give details about the device and the measurements. In Sec. III, we present a model of the device and calculate the capacitance. The experimental results are discussed in Sec. IV. Our results are summarized in Sec. V.

II. DEVICES AND MEASUREMENTS

Figure 1(a) shows the schematic of the sample. Device was defined using shallow etching technique on a two-dimensional electron gas (2DEG) formed at a GaAs/$\mathrm{Al_{0.3}Ga_{0.7}As}$ heterointerface, with sheet density 2×10^{11} cm^{-2} and mobility 1.4×10^{5} cm^{2}/V s. The area of the dot can be estimated from the lithographic size and the edge depletion lengths, yielding $S\sim1.15\ \mu\mathrm{m}^2$. The Coulomb charging energy $E_C\approx145\ \mu$eV for the dot was extracted from the temperature dependence of the width of the Coulomb resonance peak. Assuming a parabolic confinement potential in the dot, we estimate the energy level spacing $\Delta E\sim2\pi\hbar^2/m^*S\sim6\ \mu$eV, which is a very small quantity compared to the charging energy. To work in the integer quantum Hall regime, magnetic fields around 1.95 T were applied perpendicular to the 2DEG, which may modify the energy level spacing but cannot change its order of magnitude. Devices were cooled down in a dilution refrigerator with base temperature $T=20$ mK. The effective electron temperature T_e, however, is around 96 mK. We applied a small ac excitation signal $V_g(t)$ with frequency $\omega/2\pi=1.5$ GHz on the top gate and measured the linear response of the circuit from the reservoir. Measurements were conducted based on the homodyne technique, where the detected signal was amplified and multiplied with the reference signal to achieve both the in-phase and out-of-phase response of the circuit. We then used an indirect, but absolute method, based on the ac characteristics of the system and the Coulomb blockade spectroscopy [1,3], to obtain the absolute value of C_μ.

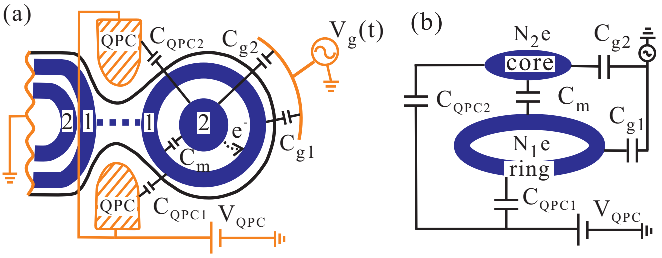

FIG. 1. (a) Schematic of the device. The bold circle on the right-hand side denotes the quantum dot and the blue strips in it indicate the compressible regions of $\mathrm{LL_1}$ and $\mathrm{LL_2}$ (indicated by 1 and 2, respectively). A gold gate is put on top of the dot and is connected to a small radio-frequency excitation voltage $V_g(t)$. Only $\mathrm{LL_1}$ in the quantum dot is tunneling coupled (indicated by the blue dotted line) to the reservoir through the quantum point contact (QPC), the transmission of which is controlled by a dc voltage V_{QPC}. C_{g1} (C_{g2}) is the capacitance between $\mathrm{LL_1}$ ($\mathrm{LL_2}$) and the top gate, and C_{QPC1} (C_{QPC2}) is the capacitance between $\mathrm{LL_1}$ ($\mathrm{LL_2}$) and the QPC gate. C_m denotes the inter-Landau-level capacitance. (b) Simplified electrical circuit used to calculate the electrostatic energy of the dot with charge number N_1e (N_2e) in $\mathrm{LL_1}$ ($\mathrm{LL_2}$). These two compressible regions are also referred to as the ring and the core.

III. MODEL AND THEORY

We focus in this work on the quantum Hall regime with the dot filling factor $2<\nu<3$ (smaller than the filling factor of the reservoir $\nu\approx4$). Hence, only two spin-split levels ($\mathrm{LL_1}$ and $\mathrm{LL_2}$) of the lowest Landau level (LL) remain in the dot. Due to self-consistent arrangement of the charge [24], $\mathrm{LL_1}$ and $\mathrm{LL_2}$ form two compressible regions, along the edge (ring) and in the center (core) of the dot [see Fig. 1(a)], respectively. They are spatially separated by an incompressible region which acts as a tunnel barrier, and electrons on these two compressible regions can transfer between each other by tunneling. Note that we are interested in the low transmission regime where only states belonging to $\mathrm{LL_1}$ are coupled to the reservoir. Hence, electrons in $\mathrm{LL_2}$ mainly influence the dot potential and can only tunnel out to the reservoir indirectly through internal charge transfer process. Therefore, it is reasonable to neglect the dynamic effect of $\mathrm{LL_2}$ and only consider its electrostatic influence. Consequently, the equivalent circuit with a series connection of a charge relaxation resistance R_q and an electrochemical capacitance C_μ is still valid.

Recent experiments [3] show that if the interactions are not too strong, i.e., $E_C\approx\Delta E$, the change of C_μ is small and the charging energy can still be taken into account, by simply replacing ΔE with $\Delta E + E_C$. For strong interactions ($E_C \gg \Delta E$), however, a recent theory predicted that electron-electron interactions may affect the density of states and lead to charge excitations [23], which may then strongly affect the oscillations of C_μ. To comprehend how the charging energy influences the electrochemical capacitance, we model the capacitor as a two-coupled-dot system. The electron-electron interactions are treated using a capacitive charging model shown in Fig. 1(b). Here, we define $C_{1\,(2)}$ as the sum of all capacitance attached to LL_1 (LL_2): $C_{1(2)} = C_{\mathrm{QPC}1(2)} + C_{\mathrm{g}1(2)} + C_{\mathrm{m}}$. The electrostatic energy of the system is the sum of the electrostatic energy stored on these two Landau levels and can be conveniently expressed using the capacitance matrix [29]. For the case with charge $Q_{1\,(2)} = -N_{1\,(2)}|e|$ in LL_1 (LL_2) and a QPC voltage V_{QPC}, we denote the electrostatic energy as $U(N_1,N_2,V_{\mathrm{QPC}})$ [see Eq. (A4) in the Appendix]. Then, the total Hamiltonian of the system is

$$H = H_L + H_D + \sum_{k,m} (t_{km} c_k^\dagger d_m + \mathrm{H.c.}), \tag{2}$$

where $H_L = \sum_k \epsilon_k c_k^\dagger c_k$ describes the electrons in the lead and the third term describes the tunneling Hamiltonian between the dot states and the lead states. The Hamiltonian of the dot reads as $H_D = \sum_{m=1}^{N_1} \epsilon_{1,m}(t) d_m^\dagger d_m + U(N_1,N_2,V_{\mathrm{QPC}})$, with $\epsilon_{1,m}(t) = \epsilon_{1,m} + eU(t)$. $U(t)$ describes the time-dependent effective potential inside the dot.

The transmission through the QPC channel is small, so it is reasonable to consider the limit $t_{km} \ll \Delta\epsilon_1$, e^2/C, where $\Delta\epsilon_1$ and e^2/C represent the mean energy level spacing and the charging energy of LL_1, respectively. Therefore, in the vicinity of electron transfer resonance $(N_1,N_2) \to (N_1-1,N_2)$, we only need to consider the hybridization of the N_1th energy level in LL_1 $|1,N_1\rangle$ (the highest occupied level in LL_1) with states in the lead. Neglecting spin effects, we rewrite the Hamiltonian in Eq. (2) as

$$\begin{aligned} H = {} & \sum_k \epsilon_k c_k^\dagger c_k + [\epsilon_{1,N_1} + eU(t) + U_1 - U_2] d_{N_1}^\dagger d_{N_1} \\ & + \sum_k (t_{kN_1} c_k^\dagger d_{N_1} + \mathrm{H.c.}) \end{aligned} \tag{3}$$

plus an additive constant $E_1 = \sum_{m=1}^{N_1-1} \epsilon_{1,m} + U_2$, where $U_1 = U(N_1,N_2,V_{\mathrm{QPC}})$ and $U_2 = U(N_1-1,N_2,V_{\mathrm{QPC}})$.

Following Ref. [19] where the Hartree-Fock approximation was used to consider the interactions, we conducted a similar calculation and find the electrochemical capacitance at zero temperature

$$C_\mu = \frac{C_1 e^2 \nu(\mu_{\mathrm{res}})}{C_1 + e^2 \nu(\mu_{\mathrm{res}})}, \tag{4}$$

where $\nu(\mu_{\mathrm{res}}) = G_{\mathrm{eq}}^R(\mu_{\mathrm{res}}) \Gamma G_{\mathrm{eq}}^A(\mu_{\mathrm{res}})/2\pi$ is the interaction density of states in LL_1 at the energy of the electrochemical potential of the reservoir μ_{res}. Γ describes the level-width function of the QD due to the coupling to the reservoir. $G_{\mathrm{eq}}^{\mathrm{R}}(\mu_{\mathrm{res}})$ is the equilibrium retard Green's function which is given by

$$G_{\mathrm{eq}}^R(\mu_{\mathrm{res}}) = \frac{1}{\mu_{\mathrm{res}} - (\epsilon_{N_1} + U_1 - U_2) + i\Gamma/2 + i0^+}. \tag{5}$$

The equilibrium advanced Green's function $G_{\mathrm{eq}}^A(\mu_{\mathrm{res}})$ is the complex conjugate of $G_{\mathrm{eq}}^R(\mu_{\mathrm{res}})$ and can be easily obtained using Eq. (5). In Eq. (4), $e^2\nu(\mu_{\mathrm{res}})$ is also referred to as the quantum capacitance C_q. Hence, the electrochemical capacitance C_μ is actually a series combination of the geometric capacitance C_1 and the quantum capacitance C_q.

To understand how the charging energy influences the capacitance, we introduce the electrochemical potential of the compressible region which is defined as the energy needed to add one electron to it. Considering both the single-level energy and the electrostatic energy, we find the electrochemical potential to add the N_1th electron to LL_1: $\mu_1(N_1,N_2) = \epsilon_{N_1} + U_1 - U_2$. It describes the position of the N_1th energy level in LL_1, which is modified by the charging energy. Therefore, Eq. (5) can be rewritten as

$$G_{\mathrm{eq}}^R(\mu_{\mathrm{res}}) = \frac{1}{\mu_{\mathrm{res}} - \mu_1(N_1,N_2) + i\Gamma/2 + i0^+}. \tag{6}$$

In Eq. (6), we define $\delta E = \mu_{\mathrm{res}} - \mu_1(N_1,N_2)$ which denotes the energy difference between the highest occupied level in LL_1 and the electrochemical potential of the reservoir. When $\delta E = 0$, one energy level in LL_1 is in resonance with the reservoir and the electrochemical capacitance C_μ reaches maximum. When δE is large, the dot level is off resonance and C_μ has a smaller value. In short, on changing the dot potential, C_μ should still oscillate periodically. Moreover, we demonstrate that, in this low transmission regime, the strong electron-electron interactions are still reasonably considered by simply modifying the oscillation periodicity with the charging energy. Therefore, we can still consider the density of states of the energy level instead of that of the charge excitations.

Note that by far we have not considered the temperature effects. For the fermion system at finite temperature, the occupation probability of the energy levels is given by the Fermi-Dirac distribution. To consider this temperature effect, we have to replace $\nu(\mu_{\mathrm{res}})$ in Eq. (4) with an effective density of states $\widetilde{\nu}(\epsilon)$, which is given by the convolution between the zero-temperature density of states $\nu(\epsilon)$ and the derivative of the Fermi-Dirac distribution with respect to energy $(-df/d\epsilon)$:

$$\widetilde{\nu}(\epsilon) = \int d\epsilon\, \nu(\epsilon) \left(-\frac{df}{d\epsilon}\right). \tag{7}$$

The shape of $(-df/d\epsilon)$ as a function of energy ϵ is shown in Fig. 3(b). It peaks at μ_{res} and has a thermal width that is proportional to $k_B T_{\mathrm{e}}$, where k_B is the Boltzmann constant. It indicates that only energy levels in this energy range may have occupation probability variations and lead to the resonance peak of C_μ.

To proceed further, we calculate the electrochemical potential using the electrostatic energy relation [see Eq. (A4) in the Appendix], which gives

$$\begin{aligned} \mu_1(N_1,N_2) = {} & \epsilon_{1,N_1} + (N_1 - 1/2)E_{C1} + N_2 E_{Cm} \\ & - \frac{V_{\mathrm{QPC}}}{|e|}(C_{\mathrm{QPC}1} E_{C1} + C_{\mathrm{QPC}2} E_{Cm}). \end{aligned} \tag{8}$$

Similarly, the electrochemical potential $\mu_2(N_1,N_2)$ of LL_2 can also be obtained by replacing all the subscripts 1 (2) on the right of Eq. (8) with 2 (1). Here, the energy ϵ_{1,N_1} (ϵ_{2,N_2}) of a single-particle energy level in LL_1 (LL_2) is a sensitive function of the magnetic field B. For a parabolic confinement, which is a good approximation for the real dot confinement [24,26], the energy spectrum is given by the Fock-Darwin spectrum [31]. For our strong magnetic fields ($\omega_c \gg \omega_0$), the energy is simplified to $\epsilon_{i,N_i} = 1/2\hbar\omega_c + N_i\Delta\epsilon_i$ $(i = 1,2)$, where $\omega_c = eB/m^*$ is the cyclotron frequency, m^* is the effective mass in GaAs, ω_0 characterizes the parabolic confinement, and $\Delta\epsilon_1 = \Delta\epsilon_2 \approx \hbar\omega_0^2/\omega_c$ is the energy separation between adjacent states in the same Landau level. $\Delta\epsilon_i$ is actually a function of B, however, it varies very slowly and can be treated as a constant in the small field range we are interested in. The spin-splitting energy in GaAs is very small compared to the cyclotron energy $\hbar\omega_c$ and is neglected throughout this paper. The only spin effect that needs to be considered is the formation of two spatially separated compression regions. $E_{C1\,(2)}$ represents the equivalent charging energy of LL_1 (LL_2) when one extra electron is added to it from the reservoir and E_{Cm} denotes the equivalent charging energy of LL_1 (LL_2) when one extra electron is added to LL_2 (LL_1) from the reservoir [see Eq. (A7) in the Appendix]. An interesting fact inferred from Eq. (8) is that the electrochemical potential μ_1 depends on both N_1 and N_2, due to internal capacitive coupling. Moreover, both N_1 and N_2 can be tuned by the QPC voltage V_{QPC} and the magnetic field B. Considering that the electrocapacitance C_μ depends sensitively on μ_1 as shown in Eqs. (4) and (6), we can then employ V_{QPC} and B to modulate C_μ.

The electrochemical potential change for different number and distribution of electrons inside the QD can be easily extracted from Eq. (8). To transfer one electron from LL_1 to the reservoir, the electrochemical potential of it changes by $E_1 = \mu_1(N_1,N_2) - \mu_1(N_1 - 1,N_2)$, which gives $E_1 = E_{C1} + \Delta\epsilon_1$. Similarly, to transfer one electron from LL_2 to the reservoir, μ_2 changes by $E_2 = E_{C2} + \Delta\epsilon_2$. Meanwhile, when a electron transfers from one LL to the reservoir, the electrochemical potential in the other LL changes by $E_{\text{m}} = \mu_1(N_1,N_2) - \mu_1(N_1,N_2 - 1) = \mu_2(N_1,N_2) - \mu_2(N_1 - 1,N_2) = E_{Cm}$. For the internal charging process, e.g., one electron transfers from LL_2 to LL_1, the electrochemical potential difference of LL_1 is $E_{\text{in}} = \mu_1(N_1 + 1,N_2 - 1) - \mu_1(N_1,N_2)$, which gives us $E_{\text{in}} = E_{C1} + \Delta\epsilon_1 - E_{\text{m}}$.

IV. RESULTS AND DISCUSSION

A typical structure of the response for a two-coupled-dot system is its charge stability diagram [29], which shows the equilibrium charge number in each dot and allows us to extract the characteristic energy scales of the double dot. Here, we set up such a diagram by measuring the electrochemical capacitance and employing the QPC voltage and the magnetic field to modulate the electron number and their distribution inside the dot. Figure 2(a) shows a color scale plot of the electrochemical capacitance C_μ as a function of V_{QPC} and B. The Coulomb resonance peaks are indicated by dashed lines, which show sawtoothlike manner along the magnetic field axis. By connecting the adjacent turning points between different Coulomb peaks, we obtain the charge stability diagram with a characteristic honeycomb structure [Fig. 2(b)]. Within each honeycomb cell, the electron numbers on both compressible regions are well defined due to Coulomb blockade.

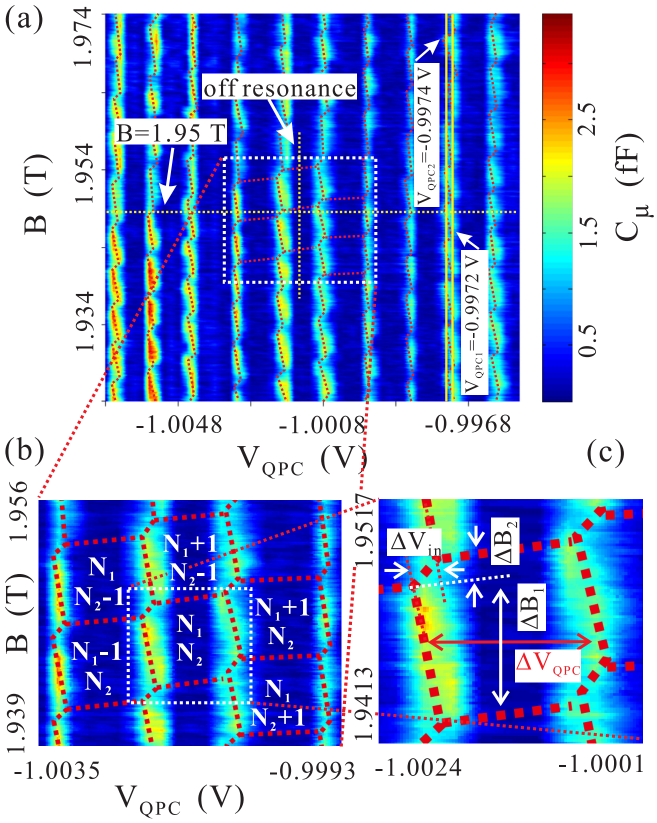

FIG. 2. (a) Electrochemical capacitance oscillations, measured as a function of QPC voltage V_{QPC} and magnetic field B. The red dashed lines indicate the positions of the peaks. (b) The charge stability diagrams are formed by connecting the adjacent turning points between different Coulomb peaks. Each cell is given by (N_1,N_2), where N_i $(i = 1,2)$ denotes the number of electrons in LL_i. (c) One cell showing the voltage and magnetic field intervals due to different energy spacings when the number or distribution of electrons in the dot is changed. Their relations are given in Eqs. (9), (10), (11), and (12).

Different from the experiments with two spin-degenerate Landau levels [30,31], where a single-particle picture such as the Fock-Darwin spectrum is enough to understand the structure of the charge stability program, in our experiment, extra consideration must be taken in understanding this structure. Since, as we discussed earlier in the single-particle picture, the two spin-split states of the lowest Landau level both increase with B, which does not lead to any frequent energy level crossings. Instead, we have to consider the self-consistent distribution of charge density and the related electrostatic potential modulation [24]. In the self-consistent model [24], increasing B makes the edge of the compressible region move from dot edge to center. Before internal electron redistribution, the electron density therefore rises in the center of the dot and decreases at the edge, thereby increasing μ_2 and decreasing μ_1 [see Fig. 3(a)]. This magnetic field dependence of the electrochemical potential can be well characterized by adding a linear term $\beta_{1(2)}B$ to the electrochemical potential $\mu_{1(2)}$ in Eq. (8). Further increasing B, when the occupied energy level $\mu_2(N_1,N_2)$ aligns with the unoccupied energy level $\mu_1(N_1 + 1, N_2 - 1)$ as shown in Fig. 3(a), the electron will transfer from

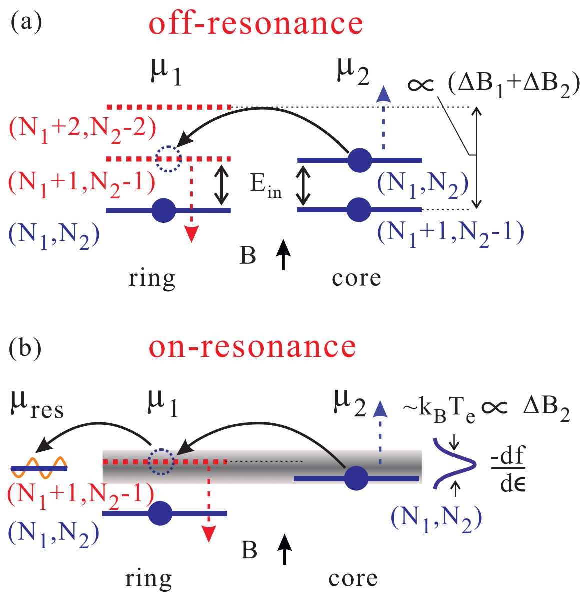

FIG. 3. Energy level diagram showing how magnetic field B modulates internal charge distribution when energy levels are (a) off resonance [indicated by a short yellow line in Fig. 2(a)] and (b) on resonance. μ_1 and μ_2 denote the electrochemical potentials of LL_1 and LL_2, respectively. Numbers in the parentheses represent the electron numbers in LL_1 (former) and LL_2 (later). E_{in} denotes the energy change when internal charge transfer happens. The shadowed area around μ_{res} in (b) represents the thermal broadening of the effective density of states ($\sim k_B T_e \approx 8\ \mu$eV).

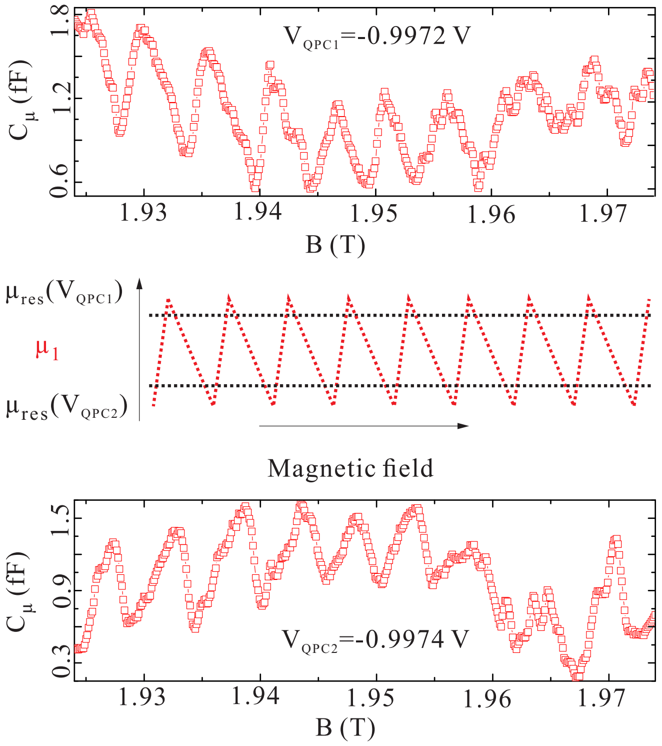

FIG. 4. The top and bottom parts: oscillations of the electrochemical capacitance C_μ as a function of magnetic field B for two quantum point contact voltages [indicated by two vertical yellow lines in Fig. 2(a)]. The middle parts: schematic of sawtooth-shaped oscillations of μ_1 on increasing B for two quantum point contact voltages. The position of the reservoir electrochemical potential μ_{res} relative to μ_1 is indicated by two dotted black lines.

the core to the ring. Continue to increase B, the next internal charge transfer happens when $\mu_2(N_1+1,N_2-1)$ aligns with $\mu_1(N_1+2,N_2-2)$. Therefore, between the two successive internal charge transfer processes, the magnetic field change $\Delta B_1 + \Delta B_2$ corresponds an energy variation $2E_{in}$. We will use this relation to extract the rate of electrochemical potential change in the later calculation [see Eq. (12)].

The bright peaks in Fig. 2(a) correspond to the direct charge tunneling from the on-resonance energy levels in LL_1 to the reservoir. The peak positions, therefore, reflect the positions of energy levels in LL_1, and we can use their magnetic field dependence to extract the parameter β_1 [see Eq. (11)]. The dark peaks, on the other hand, reflect the indirect charge transfer from the core to the reservoir via the ring levels. As shown in Fig. 3(b), when the highest occupied energy level $\mu_2(N_1,N_2)$ and the lowest unoccupied energy level $\mu_1(N_1+1,N_2-1)$ enter the thermal broadening region (the shadowed area around μ_{res}), the electron can move from LL_2 to LL_1 with thermal excitation and then tunnel out into the reservoir. The dark peak positions, therefore, do not reflect the exact positions of energy levels in LL_1 or LL_2, but reflect the peak positions of the combination of their effective density of states. Further increasing B, the internal charge transfer continues until the two energy levels move out of the thermal broadening region, and the occupation probability of the earlier lowest unoccupied energy level $\mu_1(N_1+1,N_2-1)$ now equals to one. Therefore, the small magnetic field range ΔB_2 over which the peak position increases steeply, is determined by the thermal broadening energy range around μ_{res} as well as the rate of electrochemical potential change of both μ_1 and μ_2 as a function of B. This process changes the electrostatic potential due to internal charging effect, hence, changes the bright peak positions. Therefore, we emphasize that it is more appropriate to say that Fig. 2 reflects the charge addition spectrum [24] instead of the energy level spectrum since it is the self-consistent electrostatic potential and charging effects not the single-particle energy level that dominates the structures.

Figure 4 shows the electrochemical capacitance C_μ as a function of magnetic field for two QPC voltages [their positions are indicated by two vertical lines in Fig. 2(a)], both of which show sawtoothlike structures but with reversed sawtooth directions: for $V_{QPC} = -0.9972$ V, C_μ rises steeply and falls gradually; for $V_{QPC} = -0.9974$ V, C_μ rises gradually and falls steeply. These sawtoothlike oscillations of C_μ can be easily understood in terms of the electrochemical potential μ_1 of LL_1. As inferred from the charge stability diagram in Fig. 2(a), μ_1 is modulated by B through two processes. First, before internal charge transfer, μ_1 decreases with B due to self-consistent electrostatic potential change. Second, when internal charge transfer happens, μ_1 increases steeply due to the internal charging effect. Therefore, μ_1 varies in a sawtooth manner when increasing the magnetic field. For $V_{QPC} = -0.9972$ V, μ_{res} intersects with the top half of the sawtooth structure of μ_1. On increasing the magnetic field, each time the internal charge transfer happens, μ_1 jumps towards μ_{res}, hence, C_μ

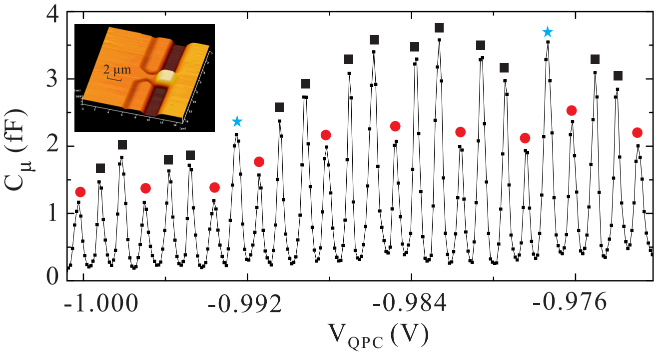

FIG. 5. Oscillations of the electrochemical capacitance as a function of $V_{\rm QPC}$ for $B = 1.95$ T [indicated by a horizontal yellow line in Fig. 2(a)]. It shows modulation of the peak amplitude, as indicated by different symbols (see more details in the text). Inset: AFM picture of the device.

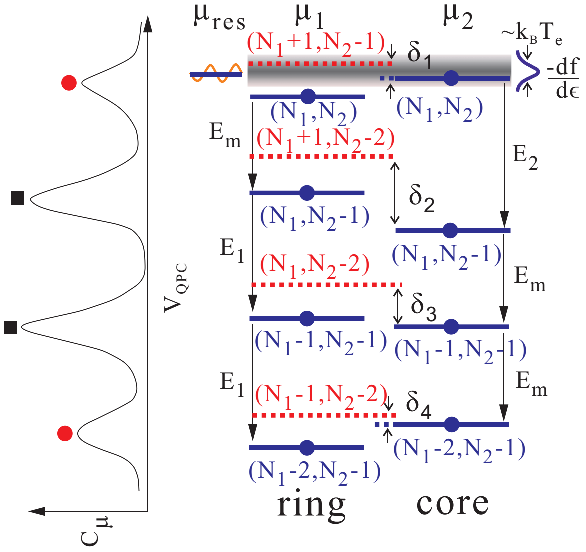

FIG. 6. Left-hand side: the related oscillation peaks of electrochemical capacitance C_μ when the quantum point contact voltage $V_{\rm QPC}$ is varied. Right-hand side: energy level diagram showing the electrochemical potentials $\mu_{\rm res}$, μ_1 and μ_2 of the reservoir LL$_1$ and LL$_2$, respectively. Numbers in the parentheses represent the electron numbers in LL$_1$ and LL$_2$. E_i ($i = 1,2$) denotes the energy change in LL$_i$ when one electron in it tunnels out and $E_{\rm m}$ denotes the energy change in one Landau level when one electron in the other Landau level tunnels out. The shadowed area around $\mu_{\rm res}$ represents the thermal broadening of the effective density of states ($\sim k_B T_{\rm e} \approx 8$ μeV).

rises steeply. When the magnetic field is further increased, μ_1 slowly drops away from $\mu_{\rm res}$ due to self-consistent electrostatic potential change, which leads to the slow C_μ decrease. For $V_{\rm QPC} = -0.9974$ V, on the other hand, $\mu_{\rm res}$ intersects with the bottom half of μ_1. On increasing B, μ_1 jumps away from $\mu_{\rm res}$ and increases slowly towards $\mu_{\rm res}$, which, consequently, reverses the orientation of the sawtooth structures of C_μ.

It is worth noting that, for some magnetic fields, $\mu_{\rm res}$ may intersect with the sawtooth structure of μ_1 at approximately its center. Hence, μ_1 may move away and toward $\mu_{\rm res}$ twice for one tooth structure of μ_1, which consequently leads to two small peaks of C_μ in one tooth. This is actually observed in Fig. 4 for both voltages at magnetic field around 1.765 T. On the other hand, as the charge relaxation time $\tau_{RC} = R_q C_\mu$ is proportional C_μ, τ_{RC} also has a sawtooth structure when the magnetic field is varied. In this respect, our experiment demonstrates how the charge dynamics is modulated by the magnetic field through internal charge transfer. Moreover, in an earlier experiment [26], the time of the internal electron transfer has been measured, which shows a macroscopic timescale and cannot be well explained in their noninteracting picture. We argue that this may due to long charge relaxation time since electron staying on one energy level for a long time can block subsequent electron transfer. Finally, for magnetic fields higher than 2.2 T, the tooth structures of C_μ disappear, which results from the fully depopulation of electrons in LL$_2$. As in this case, only one compressible region is left and no internal electron redistribution can happen. Then, we estimate the electron density inside the dot is reduced by ≈47%, compared to that in the reservoir.

Figure 5 presents the Coulomb blockade oscillations of the electrochemical capacitance as a function of $V_{\rm QPC}$ at $B = 1.95$ T, the position of which is indicated by the horizontal yellow line in Fig. 2(a). $V_{\rm QPC}$ has two effects on the sample parameters. First, it controls the transmission of the QPC. We tuned $V_{\rm QPC}$ to very negative values so as to work in the weak tunneling regime. Second, it changes the static potential of the dot linearly. By changing $V_{\rm QPC}$ continuously, each time one dot level aligns with the electrochemical potential in the reservoir, there is a peak of the capacitance oscillations. The Coulomb oscillation period only varies a little bit for this strong magnetic field compared to that in $B = 0$. It indicates that the period is dominated by the the Coulomb charging energy for our strong interacting devices, and supports our assumption of a parabolic confinement. Since for strong confinement like steep wall potentials, the period should vary enormously as the single-particle energy is large and sensitive to magnetic fields [31]. For the peak height, we find a nearly periodic amplitude modulation, with every two similar high peaks (black squares) separated by one low peak (red circle). But, there are some exceptions: after five peaks of low amplitude and four pairs of high amplitude, one peak of high amplitude (blue star) appears. From Fig. 2(a), we immediately see that the large peaks correspond to the variations of electrons in the ring, whereas the small ones correspond to these in the core.

To further understand how the internal charge transfer affects the amplitude modulation, we draw an energy diagram in Fig. 6, which illustrates the energy variations when the number of the electrons is tuned by $V_{\rm QPC}$. The left-hand side of Fig. 6 shows the electrochemical capacitance C_μ as a function of $V_{\rm QPC}$. We start with the topmost small peak of C_μ, which corresponds to the region where the energy difference δ_1 between $\mu_1(N_1+1, N_2-1)$ and $\mu_2(N_1, N_2)$ is smaller than the thermal width ($\sim k_B T_{\rm e} \approx 8$ μeV). Therefore, electron in the latter energy level can transfer to the former energy level with thermal excitation, and finally tunnels into the reservoir. Consequently, C_μ shows a resonance peak but with a small amplitude, as it is limited by the small tunneling rate of electrons from the core to the ring. This process removes an electron from the core into the reservoir and lowers μ_1 by the interaction energy E_m and μ_2 by energy E_2. In our experiment, the efficiency of V_QPC in tuning the potential is approximately the same for the core and the ring, so energy levels in both regions move with the same pace as V_QPC is varied. We decrease V_QPC to align $\mu_1(N_1+1,N_2-2)$ with μ_res. However, resonance does not occur as this level is Coulomb blocked, and electron in the core cannot transfer to this ring level because the energy difference δ_2 is too large compared to the thermal excitation. The next resonance happens only when $\mu_1(N_1,N_2-1)$ lines up with μ_res, and the electron on this ring level can transfer directly to the reservoir, which gives a large peak of C_μ and lowers μ_1 by E_1 and μ_2 by E_m. Continuing to decrease V_QPC, similar process happens for the next resonance and another high peak is observed. However, since $E_1 > E_\mathrm{m}$, after this peak the core level $\mu_2(N_1-2,N_2-1)$ becomes higher than the ring level $\mu_1(N_1-2,N_2-1)$, and the energy difference δ_4 between $\mu_2(N_1-2,N_2-1)$ and $\mu_1(N_1-1,N_2-2)$ is comparable to the thermal width again. Electron will transfer from the core to the reservoir via the ring level and we will have another small peak. All the above processes can be treated as one period and electrochemical capacitance peaks show a nearly periodic amplitude modulation.

The exceptions of the amplitude modulation can also be well explained in our model. As shown in Fig. 6, for the second low peak the energy difference δ_4 is actually smaller than δ_1, which will decrease the energy differences, δ_i $(i=1,2,3,4)$, for the next amplitude modulation period. Such decrease continues for another two more amplitude modulation periods until δ_3 becomes comparable to the thermal expansion width. Then, indirect electron transfer will happen and the second large peak will become a small one. In addition, this small peak becomes the start of next regular amplitude modulation period. Consequently, we see the exceptions in Fig. 5, where only one large peak is observed between two small ones.

For a quantitative understanding of the experimental results, we next try to obtain the various charging energy scales and their parameter dependence employing our earlier theoretical results. One honeycomb cell is shown in Fig. 2(c). The magnetic field mainly redistributes electrons between the two compressible regions and only slightly changes the tunneling rate, while the QPC voltage mainly changes the total electron population in the dot. Therefore, the almost horizontal lines correspond to the transfer of electrons from the core to the ring, whereas the almost vertical lines indicate changes in the electron number on the QD. The period to add one extra electron to the dot is $\Delta V_\mathrm{QPC} = 1.01$ mV. To transfer one electron from the core to the ring, the corresponding energy change of μ_1 is related to a small QPC voltage change $\Delta V_\mathrm{in} = 0.163$ mV. Using Eq. (8), we then find the relation between the voltage (field) scales of the honeycomb and the charging energy. From

$$\mu_1(N_1,N_2,V_\mathrm{QPC},B) = \mu_1(N_1+1,N_2,V_\mathrm{QPC}+\Delta V_\mathrm{QPC},B)$$

we obtain

$$\Delta V_\mathrm{QPC} = \frac{|e|E_1}{C_\mathrm{QPC1}E_{C1} + C_\mathrm{QPC2}E_{Cm}}. \tag{9}$$

From

$$\mu_1(N_1,N_2,V_\mathrm{QPC},B) = \mu_1(N_1+1,N_2-1,V_\mathrm{QPC}+\Delta V_\mathrm{in},B)$$

we obtain

$$\Delta V_\mathrm{in} = \frac{|e|E_\mathrm{in}}{C_\mathrm{QPC1}E_{C1} + C_\mathrm{QPC2}E_{Cm}}. \tag{10}$$

Using the temperature dependence of the width of the Coulomb resonance peaks [1], we obtain the QPC gate voltage and dot electrochemical potential transferring parameter $\alpha = 0.144$ eV/V, which is defined by $\alpha\Delta V_\mathrm{QPC} = E_1$. Combining it with Eqs. (9) and (10), we find that the single-particle charging energy $E_1 = E_{C1} + \Delta\epsilon_1 \approx 145\ \mu$eV, $E_\mathrm{in} \approx 23\ \mu$eV, and $E_\mathrm{m} = E_1 - E_\mathrm{in} \approx 122\ \mu$eV. From the nearly periodic amplitude modulation and the related energy diagram in Fig. 6(c), we have $E_\mathrm{m} + 2E_1 \approx E_2 + 2E_\mathrm{m}$, which gives $E_2 = E_{C2} + \Delta\epsilon_2 \approx 169\ \mu$eV.

For the magnetic field dependence of μ_1, our earlier analysis show that the slope $d\mu_1/dB$ is composed of two contributions, i.e., the single-particle energy level part $\hbar e/2m^*$ and the self-consistent potential part β_1 ($d\mu_2/dB$ has two similar contributions). With the magnetic field range obtained in Fig. 2(c), we have

$$\Delta B_1(\beta_1 + \hbar e/2m^*) = -E_\mathrm{in}. \tag{11}$$

We then obtain the linear coefficient between the field and the potential μ_1, $\beta_1 \approx -6.6$ meV T^{-1}, which is much larger than $\hbar\omega_c/B$ (1.76 meV T^{-1}). It indicates that the internal electrostatic potential in the dot is a very sensitive function of magnetic field. In our earlier analysis, we also found that between two successive internal charge transfer processes, the magnetic field variation $\Delta B_1 + \Delta B_2$ corresponds an energy variation $2E_\mathrm{in}$:

$$\begin{aligned}(\Delta B_1 + \Delta B_2)&(d\mu_2/dB - d\mu_1/dB)\\ &= (\Delta B_1 + \Delta B_2)(\beta_2 - \beta_1) = 2E_\mathrm{in}.\end{aligned} \tag{12}$$

Using the value of β_1 obtained from Eq. (11), we then obtain the linear coefficient between the field and the potential μ_2, $\beta_2 \approx 2.9$ meV T^{-1}, which is much smaller than β_1. One possible explanation is that the charge density varies slower in the center than that in the edge when B is changed. In Fig. 2(c), we also have a smaller magnetic field range ΔB_2, which corresponds to the internal charge transfer process. It is determined by the thermal width as well as the slope of both μ_1 and μ_2, i.e., $\Delta B_2(\beta_2 - \beta_1) \sim k_B T_\mathrm{e}$. Combining with the obtained values of β_1 and β_2, we then estimate the effective electron temperature $T_\mathrm{e} \sim 90$ mK, which agrees remarkably well with the value (96 mK) obtained from the Coulomb blockade spectrum.

As the energy change of the electrochemical potential is directly related to the geometric capacitance elements [see Eq. (A7) in Appendix], we next use it to roughly estimate these capacitance elements and the related spatial extent of the compressible and incompressible regions. For simplicity, we neglect the mean single-level spacing $\Delta\epsilon_i \approx \hbar\omega_0^2/\omega_c$, which is appropriate as ω_0 for our large dot is very small compared to ω_c. Using the charge energy obtained earlier and the energy-capacitance relations [see Eq. (A7) in Appendix], we find that the internal capacitance $C_\mathrm{m} \approx 2$ fF, which is much larger compared to former experiments with two spin-degenerate Landau levels [31]. This implies that the two spin-split Landau levels have stronger capacitive coupling and offers us a way to investigate the effects of strong electron interactions between different Landau levels affecting the transport. In addition, we find $C_{\mathrm{G1}} = C_{\mathrm{g1}} + C_{\mathrm{QPC1}} \approx 0.77$ fF and $C_{\mathrm{G2}} = C_{\mathrm{g2}} + C_{\mathrm{QPC2}} \approx 0.38$ fF. Hence, the outer compressible region is approximately twice the area of the inner compressible region if we assume the capacitance is proportional to the plate area. We denote the width of the incompressible region, the outer compressible region, and the inner compressible region by w_0, w_1, and w_2, respectively. The radius of the outer compressible region is assumed to be the same as that of the dot which is $r \sim 0.6$ μm. Then, we use the capacitance formula for a coplanar capacitor [27,31] to estimate the ratio $w_1/w_0 = \frac{1}{4}\exp(C_{\mathrm{m}}/4\varepsilon_r\varepsilon_0 r) \approx 335$, with $\varepsilon_r = 13$ for GaAs and ε_0 being the vacuum permittivity. Considering the area ratio ($\sim$2) of the two compressible regions, we finally find $w_0 \approx 1$ nm, $w_1 \approx 267$ nm, and $w_2 \approx 332$ nm. The incompressible region is one order of magnitude smaller than former estimation with two spin-degenerate Landau levels [31]. This indicates that the spatial separation between the two compressible regions due to the spin-split energy ($\sim g\mu_B B$) is much smaller than that due to the cyclotron energy ($\sim\hbar\omega_c$). Therefore, one advantage of this system, compared to the real double-dot devices, is that the internal coupling is much stronger, and it enables us to investigate how interactions influence the dynamics of single electrons on a much smaller spatial scale. Moveover, the two compressible regions in our case have comparable widths as they are from the same Landau level, while for the two spin-degenerate Landau levels, the inner region was found to be much larger than the outer region [31,32]. This further strengthens the internal capacitive coupling between Landau levels. According to a previous theory [33], the width of the outer compressible regime w_1 is directly related to the potential profile $w_1 \propto [dn(x)/dx]^{-1}$, where $n(x)$ is the total electron density and x is the distance from the dot edge. Considering that $dn(x)/dx$ is proportional to the electric field at x, the large w_1 then corresponds to a small electric field, i.e., a slow spatial variation rate of potential, which agrees with our charge-density model with a parabolic confinement.

V. CONCLUSION

In conclusion, we have measured the electrochemical capacitance of an interacting mesoscopic capacitor in the quantum Hall regime. We focused on the weak tunneling regime where electrons are quantized on two well-separated compressible regions inside the dot and can transfer between these two regions. We found that both the periodicity and amplitudes of the electrochemical capacitance oscillations are modified by the charging energy and the internal electron distribution, when the voltage of the quantum point contact and the magnetic field are swept. The charge stability diagram of the electrochemical capacitance shows a honeycomb shape, which, together with all other capacitance properties, is well understood by including the interactions with a two-dot charging model. Our measurements indicate that the internal capacitive coupling between the two confined spin-split levels is strong and their electrostatic potential is sensitive to magnetic field. As the charge relaxation time is proportional to the electrochemical capacitance, we further infer that the dynamic of single electrons also depends sensitively on the internal charge transfer. The demonstrated technique is of interest as a tool for fast and sensitive charge state readout and may have important application in fermion-based quantum information processing [34,35]. Operated out of equilibrium by a sudden voltage, capacitor with strong Coulomb interaction was predicted to have different relaxation time of charge and spin [36], and can emit a sequence of multiple charge pulses [15]. Moreover, many new effects due to strong interaction may emerge in quantum electron optic experiments [10–12]. We hope that this work will stimulate further research in these fields as well as the research in the self-consistent calculations of dot potential for the dynamic transport.

ACKNOWLEDGMENTS

This research is supported by the National Key Research and Development Program of China under Grant No. 2016YFF0200403 and the State Key program of National Natural Science of China under Grant No. 11234009.

APPENDIX

In this appendix, we derive the electrostatic energy of double-quantum-dot system. The total charge $Q_{1(2)}$ on dot 1 (2) as the sum of the charges on all the capacitors connected to dot 1 (2) can be written as

$$\begin{aligned} Q_1 &= C_{\mathrm{g1}}V_1 + C_{\mathrm{m}}(V_1 - V_2) + C_{\mathrm{QPC1}}(V_1 - V_{\mathrm{QPC}}),\\ Q_2 &= C_{\mathrm{g2}}V_2 + C_{\mathrm{m}}(V_2 - V_1) + C_{\mathrm{QPC2}}(V_2 - V_{\mathrm{QPC}}). \end{aligned} \tag{A1}$$

We can rewrite it as

$$\begin{pmatrix} Q_1 + C_{\mathrm{QPC1}}V_{\mathrm{QPC}} \\ Q_2 + C_{\mathrm{QPC2}}V_{\mathrm{QPC}} \end{pmatrix} = \begin{pmatrix} C_1 & -C_{\mathrm{m}} \\ -C_{\mathrm{m}} & C_2 \end{pmatrix}\begin{pmatrix} V_1 \\ V_2 \end{pmatrix}, \tag{A2}$$

where $C_1 = C_{\mathrm{m}} + C_{\mathrm{g1}} + C_{\mathrm{QPC1}}$ and $C_2 = C_{\mathrm{m}} + C_{\mathrm{g2}} + C_{\mathrm{QPC2}}$. Using the above expression, we can write voltages on the quantum dots as

$$\begin{pmatrix} V_1 \\ V_2 \end{pmatrix} = \frac{1}{C_1C_2 - C_{\mathrm{m}}^2}\begin{pmatrix} C_2 & C_{\mathrm{m}} \\ C_{\mathrm{m}} & C_1 \end{pmatrix}\begin{pmatrix} Q_1 + C_{\mathrm{QPC1}}V_{\mathrm{QPC}} \\ Q_2 + C_{\mathrm{QPC2}}V_{\mathrm{QPC}} \end{pmatrix}. \tag{A3}$$

The electrostatic energy of the double-dot system is the sum of the electrostatic energy stored on the dots and can be conveniently expressed using the capacitance matrix $U = \frac{1}{2}\overrightarrow{V}\cdot\overrightarrow{Q}$. For the case $Q_{1\,(2)} = -N_{1\,(2)}|e|$ this becomes

$$\begin{aligned} U(N_1,N_2,V_{\mathrm{g}},V_{\mathrm{QPC}}) = {}& \frac{1}{2}N_1^2E_{C1} + \frac{1}{2}N_2^2E_{C2} + N_1N_2E_{Cm}\\ &+ f_1(V_{\mathrm{QPC}}) + f_2(V_{\mathrm{QPC}},N_1,N_2), \end{aligned} \tag{A4}$$

$$\begin{aligned} f_1(V_{\mathrm{QPC}}) = {}& +\frac{V_{\mathrm{QPC}}^2}{2e^2}(C_{\mathrm{QPC1}}^2E_{C1} + C_{\mathrm{QPC2}}^2E_{C2}\\ &+ 2C_{\mathrm{QPC1}}C_{\mathrm{QPC2}}E_{Cm}), \end{aligned} \tag{A5}$$

$$\begin{aligned} f_2(V_{\mathrm{QPC}},N_1,N_2) = {}& \frac{V_{\mathrm{QPC}}}{-|e|}[C_{\mathrm{QPC1}}(N_1E_{C1} + N_2E_{Cm})\\ &+ C_{\mathrm{QPC2}}(N_1E_{Cm} + N_2E_{C2})], \end{aligned} \tag{A6}$$

where

$$E_{C1} = \frac{e^2}{C_1}\frac{1}{1-\frac{C_\mathrm{m}^2}{C_1C_2}}, \quad E_{C2} = \frac{e^2}{C_2}\frac{1}{1-\frac{C_\mathrm{m}^2}{C_1C_2}}, \quad E_{Cm} = \frac{e^2}{C_\mathrm{m}}\frac{1}{\frac{C_1C_2}{C_\mathrm{m}^2}-1}. \tag{A7}$$

---

[1] J. Gabelli, G. Fève, J.-M. Berroir, B. Plaçais, A. Cavanna, B. Etienne, Y. Jin, and D. C. Glattli, Science **313**, 499 (2006).

[2] G. Fève, A. Mahé, J.-M. Berroir, T. Kontos, B. Plaçais, D. C. Glattli, A. Cavanna, B. Etienne, and Y. Jin, Science **316**, 1169 (2007).

[3] J. Gabelli, G. Fève, J.-M. Berroir, and B. Plaçais, Rep. Prog. Phys. **75**, 126504 (2012).

[4] E. Bocquillon, V. Freulon, J.-M. Berroir, P. Degiovanni, B. Plaçais, A. Cavanna, Y. Jin, and G. Fève, Science **339**, 1054 (2013).

[5] J. Xia, F. Chen, J. Li, and N. Tao, Nat. Nanotechnol. **4**, 505 (2009).

[6] L. Li, C. Richter, S. Paetel, T. Kopp, J. Mannhart, and R. C. Ashoori, Science **332**, 825 (2011).

[7] B. Skinner and B. I. Shklovskii, Phys. Rev. B **82**, 155111 (2010).

[8] B. Skinner and B. I. Shklovskii, Phys. Rev. B **87**, 035409 (2013).

[9] G. L. Yu, R. Jalil, B. Belle, A. S. Mayorov, P. Blake, F. Schedin, S. V. Morozov, L. A. Ponomarenko, F. Chiappini, S. Wiedmann *et al.*, Proc. Natl. Acad. Sci. USA **110**, 3282 (2013).

[10] A. Mahé, F. D. Parmentier, E. Bocquillon, J.-M. Berroir, D. C. Glattli, T. Kontos, B. Plaçais, G. Fève, A. Cavanna, and Y. Jin, Phys. Rev. B **82**, 201309 (2010).

[11] F. D. Parmentier, E. Bocquillon, J.-M. Berroir, D. C. Glattli, B. Plaçais, G. Fève, M. Albert, C. Flindt, and M. Büttiker, Phys. Rev. B **85**, 165438 (2012).

[12] E. Bocquillon, F. D. Parmentier, C. Grenier, J.-M. Berroir, P. Degiovanni, D. C. Glattli, B. Plaçais, A. Cavanna, Y. Jin, and G. Fève, Phys. Rev. Lett. **108**, 196803 (2012).

[13] M. Büttiker, H. Thomas, and A. Prêtre, Phys. Lett. A **180**, 364 (1993).

[14] E. Pallecchi, A. C. Betz, J. Chaste, G. Fève, B. Huard, T. Kontos, J.-M. Berroir, and B. Plaçais, Phys. Rev. B **83**, 125408 (2011).

[15] D. Litinski, P. W. Brouwer, and M. Filippone, Phys. Rev. B **96**, 085429 (2017).

[16] J. Wang, B. Wang, and H. Guo, Phys. Rev. B **75**, 155336 (2007).

[17] Y. Yin, Phys. Rev. B **90**, 045405 (2014).

[18] R. C. Ashoori, H. L. Stormer, J. S. Weiner, L. N. Pfeiffer, K. W. Baldwin, and K. W. West, Phys. Rev. Lett. **71**, 613 (1993).

[19] S. E. Nigg, R. López, and M. Büttiker, Phys. Rev. Lett **97**, 206804 (2006).

[20] Y. Hamamoto, T. Jonckheere, T. Kato, and T. Martin, Phys. Rev. B **81**, 153305 (2010).

[21] C. Mora and K. Le Hur, Nat. Phys. **6**, 697 (2010).

[22] M. Büttiker and S. E. Nigg, Nanotechnology **18**, 044029 (2007).

[23] M. Filippone and C. Mora, Phys. Rev. B **86**, 125311 (2012).

[24] P. L. McEuen, E. B. Foxman, J. Kinaret, U. Meirav, M. A. Kastner, N. S. Wingreen, and S. J. Wind, Phys. Rev. B **45**, 11419(R) (1992).

[25] J. M. Kinaret and N. S. Wingreen, Phys. Rev. B **48**, 11113 (1993).

[26] N. C. van der Vaart, M. P. de Ruytervan Steveninck, L. P. Kouwenhoven, A. T. Johnson, Y. V. Nazarov, C. J. P. M. Harmans, and C. T. Foxon, Phys. Rev. Lett **73**, 320 (1994).

[27] A. K. Evans, L. I. Glazman, and B. I. Shklovskii, Phys. Rev. B **48**, 11120 (1993).

[28] M. Büttiker and C. A. Stafford, Phys. Rev. Lett. **76**, 495 (1996).

[29] W. G. Van der Wiel, S. De Franceschi, J. M. Elzerman, T. Fujisawa, S. Tarucha, and L. P. Kouwenhoven, Rev. Mod. Phys. **75**, 1 (2002).

[30] P. L. McEuen, E. B. Foxman, U. Meirav, M. A. Kastner, Y. Meir, N. S. Wingreen, and S. J. Wind, Phys. Rev. Lett. **66**, 1926 (1991).

[31] A. Fuhrer, S. Lüscher, T. Heinzel, K. Ensslin, W. Wegscheider, and M. Bichler, Phys. Rev. B **63**, 125309 (2001).

[32] S. Baer, C. Rösler, T. Ihn, K. Ensslin, C. Reichl, and W. Wegscheider, New J. Phys. **15**, 023035 (2013).

[33] D. B. Chklovskii, B. I. Shklovskii, and L. I. Glazman, Phys. Rev. B **46**, 4026 (1992).

[34] D. Loss and D. P. DiVincenzo, Phys. Rev. A **57**, 120 (1998).

[35] S. E. Nigg and M. Büttiker, Phys. Rev. Lett **102**, 236801 (2009).

[36] J. Splettstoesser, M. Governale, J. König, and M. Büttiker, Phys. Rev. B **81**, 165318 (2010).